GEOLOGICA CARPATHICA, 2026, 77, 1, 3–15 https://doi.org/10.31577/GeolCarp.2026.02

Spessartine nodules with hematite-rich epidote–piemontite aureoles from the RHV-1 borehole near Rudňany (north Gemeric Unit, Slovakia)

PAVOL MYŠĽAN[1,✉], MARTIN ŠTEVKO[1,2] and TOMÁŠ MIKUŠ[3]

[1]Earth Science Institute v.v.i., Slovak Academy of Sciences, Dúbravská cesta 9, 841 04 Bratislava, Slovakia
[2]Department of Mineralogy and Petrology, National Museum, Cirkusová 1740, 193 00 Praha 9 – Horní Počernice, Czech Republic
[3]Earth Science Institute v.v.i., Slovak Academy of Sciences, Ďumbierska 1, 974 11 Banská Bystrica, Slovakia

(Manuscript received October 28, 2025; accepted in revised form January 30, 2026; Associate Editor: Peter Bačík)

Abstract: Metamorphosed manganese mineralisation from the RHV-1 borehole near Rudňany (northern Gemeric Unit, Western Carpathians, Slovakia) occurs in the form of synsedimentary Mn nodules up to 1 cm in size with Mn^{3+}/Fe^{3+}-rich aureoles hosted in quartz–muscovite phyllites. These nodules show internal zoning with compact yellowish spessartine-rich cores, transitional quartz–spessartine rims, and outer reddish aureoles enriched in epidote, piemontite, hematite, Mn-rich calcite, fluorapatite, and clinochlore. Spessartine represents the dominant Mn-bearing phase (78.9–90.5 mol.% Sps), formed during the Variscan prograde metamorphism under low-temperature greenschist-facies conditions (~350–450 °C). The surrounding aureole comprises of epidote and piemontite with variable Mn^{3+}/Fe^{3+} substitutions, recording metamorphic reactions under oxidising conditions and elevated fO_2, with hematite acting as the red coloration cause. Fluorapatite occurs as an important accessory phase in two generations: early As-poor fluorapatite enclosed in later As-enriched fluorapatite rims (up to 0.29 *apfu* As^{5+}) formed during recrystallisation and fluid (re)mobilisation, possibly enhanced by Alpine tectonometamorphism. Quartz, muscovite, albite, and titanite represent phases inherited from the host phyllites. The studied mineral assemblage reflects a polyphase evolution of Mn mineralisation derived from volcaniclastic-sedimentary precursors deposited in an Early Paleozoic basin. Subsequent Variscan metamorphism produced spessartine nodules and aureoles, while Alpine metamorphism caused recrystallisation, quartz veinlet formation, and As^{5+} (re)mobilisation in outer fluorapatite zones. Compared to other occurrences in the northern Gemeric Unit (e.g., Poráč), the Rudňany assemblage is prominent for its dominance of spessartine and epidote–piemontite aureoles and a different protolith composition.

Keywords: Rudňany, Gemeric Unit, manganese mineralisation, spessartine, piemontite, epidote, As-rich fluorapatite

Introduction

Metamorphosed manganese mineralisation is currently an important subject of study, as it serves as a host environment for significant accumulations of various elements incorporated within manganese-bearing minerals. Studies focusing on the mineralogical, geochemical, petrological, or ore-deposit research of manganese mineralisation containing epidote-group minerals provide important data for understanding the evolution of manganese mineralisation in the Alps, the Eastern Carpathians, and the Western Carpathians (e.g., Cenki-Tok & Chopin 2006; Cenki-tok et al. 2006; Hîrtopanu & Udubașa 2015; Kolitsch et al. 2018).

Manganese-rich assemblages represent an unusual type of mineralisation in metamorphosed volcano-sedimentary sequences within the Gemeric Unit of the Spišsko-gemerské rudohorie Mts. (Slovakia, Western Carpathians). This mineralisation is predominantly associated with metacarbonate lenses in the southern Gemeric Unit at the localities Betliar – Július (Myšľan et al. 2023; Števko et al. 2023), Smolník – Malá Hekerová (Myšľan et al. 2025a), and Čučma – Čierna baňa (Faryad 1994; Rojkovič 2001; Peterec & Ďuďa 2003; Števko et al. 2015; Radvanec & Gonda 2020). To a lesser extent, mineralisation is linked to magnetite lenses in metarhyolite volcaniclastic sequences at the Prakovce – Zimná voda (Myšľan et al. 2024). In the northern Gemeric Unit, the occurrence of manganese mineralisation is rare and has been confirmed rarely on the surface, in the form of lenses associated with metacherts in the metabasic volcanogenic rocks of the Rakovec Group at the Diely occurrence near Poráč (Myšľan et al. 2025b).

Nevertheless, from the drilling exploration in the vicinity of the Rudňany deposit, the occurrence of Mn-rich nodules is known from borehole RHV-1, which was the subject of a preliminary mineralogical study (Spišiak et al. 1989; Spišiak & Hovorka 2000), in which accumulations of piemontite and spessartine were identified. The samples of manganese nodules originate from deep exploratory drilling works at the Rudňany deposit carried out between 1980 and 1984, which were aimed at verifying the lithological development and the presence of suitable formations potentially accumulating favourable carbonate–quartz–baryte vein structures with

✉ corresponding author: Pavol Myšľan
pavol.myslan@savba.sk

CC BY NC ND

sulfides. For this purpose, two deep boreholes, RHV-1 and RHV-2, were drilled. Only RHV-1 intercepted Mn nodules within a zone approximately 22.6 meters thick, specifically at three depths: 1259.60 m, 1280.20 m, and 1282.20 m (Hudáček et al. 1984). Borehole RHV-1 (1994 m deep) was located in mountainous terrain at an elevation of 655 m, south of the village Rudňany, in the area of the Brezová Hora ridge, with GPS coordinates 48°52'31.8"N 20°40'15.6"E. Borehole RHV-2 (1323.6 m deep) was situated on the eastern slope of Stožky Hill, approximately 250 m west of the Rudňany settlement, at an elevation of 606 m (Hudáček et al. 1984).

This study provides a more detailed insight into the mineralisation of Mn-bearing nodules and expands the knowledge of this type of mineralisation at the studied locality. It compares the results with another occurrence of Mn-rich mineralisation at the Poráč–Diely within the Rakovec Group and broadens the overall genetic understanding of the formation of Mn mineralisations in the Gemeric Unit.

Geological settings and localisation of samples

Metamorphosed manganese mineralisation at the RHV-1 borehole near Rudňany occurs within Early Paleozoic, predominantly low-grade metamorphic rocks of the Gemeric Unit (Gemeric Unit) in the Spišsko-gemerské rudohorie Mountains, Eastern Slovakia (Fig. 1). The Gemeric Unit is subdivided into three lithological groups formed under different metamorphic conditions – the Klátov, Rakovec, and Gelnica Groups. The Rakovec and Gelnica Groups underwent Variscan and Alpine metamorphism under greenschist- to locally blueschist-facies conditions. The Rakovec Group predominantly comprises metabasites and quartz phyllites. The northern Gemeric Unit is moreover represented by high-grade amphibolites of the Klátov Group and low-grade rocks of the Rakovec Group (Ivan 2009; Vozárová et al. 2013; Faryad et al. 2020). Its sedimentary cover includes Carboniferous formations of the Dobšiná and Ochtiná Groups, as well as the Permian Krompachy Group (Vozárová et al. 2021; Vozárová & Šarinová 2024). Studied samples from borehole RHV-1 were drilled through the northern Gemeric Unit sequences – specifically the rock cover sequences of the Krompachy and Dobšiná Groups, as well as the Klátov and Rakovec Groups (Fig. 1).

The metamorphosed manganese mineralisation is hosted in phyllites containing quartz, albite, muscovite, and chlorite. The overlying and underlying rocks are composed of metabasic tuffs and tuffites. These rock sequences belong to the Rakovec Group, which is subdivided into the lower Smrečinka Formation, consisting of turbiditic metasandstones and metapelites with intercalated metabasalts, and the upper Sykavka Formation, dominated by metabasalts and metavolcanoclastic rocks with minor fine-grained metasediments of continental affinity (Bajaník et al. 1981; Ivan 2009). Mafic rocks and their derivatives likely formed during submarine volcanic activity, as indicated by pillow lavas, and display geochemical signatures consistent with E-MORB/OIT (Hovorka et al. 1988; Ivan 2009). These mafic rocks were generated during Ordovician rifting of the Rakovec basin, followed by

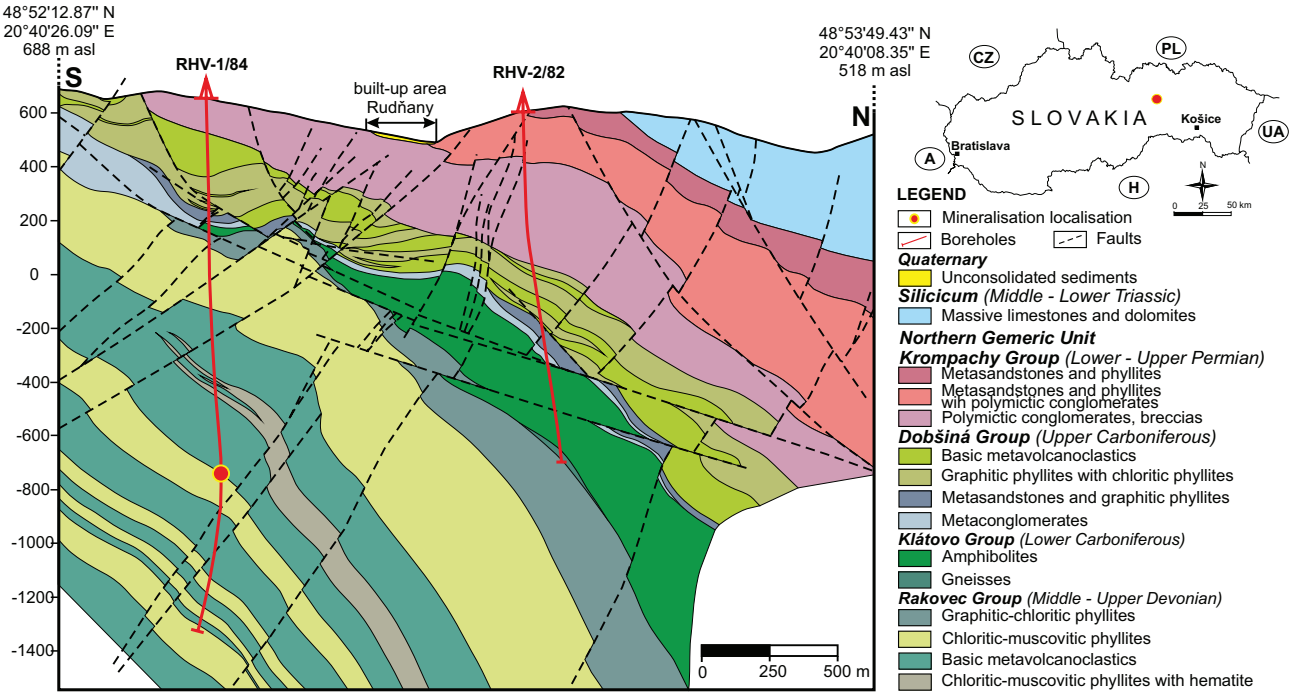

Fig. 1. Geological cross-section of the area of interest showing boreholes RHV-1 and RHV-2, with the highlighted position containing Mn-rich nodules in the metasediments of the Rakovec Group, modified after Hudáček et al. (1984).

Silurian–Carboniferous back-arc spreading and consolidation, with metamorphic evolution during the Variscan orogeny (Vozárová et al. 2013; Faryad et al. 2020). Regional metamorphism in the Rakovec Group did not exceed the lower-middle greenschist facies, with temperatures mostly between about 350 and 450 °C, as indicated by mineral assemblages in metapelites, metabasalts, and metacarbonates. The first Variscan metamorphic phase reached roughly 400–450 °C at medium to high pressures, whereas the later phase occurred at lower pressures with temperatures around 350–430 °C (Faryad 1991; Vozárová 1993).

Methods

Representative metamorphosed manganese mineralisation samples obtained from deposits at the Faculty of Natural Sciences, Comenius University in Bratislava (P. Ivan) were polished into mounts. Quantitative chemical (WDS) analyses of studied minerals were obtained using a JEOL-JXA850F field-emission electron microprobe (EMPA) in wavelength-dispersive spectrometry (WDS) mode (Earth Science Institute, Slovak Academy of Sciences, Banská Bystrica, Slovakia). The following conditions were applied: accelerating voltage 15 kV, measuring current 20 nA (silicates, carbonates). The beam diameter ranged from 3 to 10 μm, ZAF correction was used. The following standards and X-ray lines were used: albite (Al*Kα*, Na*Kα*), baryte (S*Kα*, Ba*Lα*), celestine (Sr*Lα*), $CePO_4$ (Ce*Lα*), Cr_2O_3 (Cr*Kα*), diopside (Si*Kα*, Mg*Kα*, Ca*Kα*), $DyPO_4$ (Dy*Lβ*), fluorapatite (P*Kα*), fluorite (F*Kα*), gahnite (Zn*Kα*), hematite (Fe*Kα*), $LaPO_4$ (La*Lα*), $LiNbO_4$ (Nb*Lα*), $LuPO_4$ (Lu*Lα*), $NdPO_4$ (Nd*Lα*), Ni_2Si (Ni*Kα*), orthoclase (K*Kα*), $PrPO_4$ (Pr*Lβ*), rhodonite (Mn*Kα*), rutile (Ti*Kα*), $ScVO_4$ (V*Kα*), $SmPO_4$ (Sm*Lβ*), tugtupite (Cl*Kα*), $YbPO_4$ (Yb*Lα*), and YPO_4 (Y*Lα*). The detection limit of every element ranged from 88 ppm (Ca) to 824 ppm (Zn). Elements that were analysed quantitatively and are below the detection limit are not listed in the tables. All chemical analyses are listed in Supplementary Table S1. Photographic documentation of relationships between minerals was carried out in the BSE (back-scattered electrons) mode. Mineral abbreviations used in this study are defined by Warr (2021) as follows: Ab – albite, Cal – calcite, Clc – clinochlore, Ep – epidote, Fap – fluorapatite, Hem – hematite, Ms – muscovite, Pmt – piemontite, Qz – quartz, Sps – spessartine, and Ttn – titanite.

Chemical data of epidotes were calculated on the basis of Σ(A+M+T)=8 and 12.5 oxygen atoms; if Si in the formula was Si>3.05, it was normalised again on the basis of Si=3. The Fe^{2+}/Fe^{3+} and Mn^{2+}/Mn^{3+} values were recast until Σ(cation charge) equals Σ(anion charge), oxidising first Fe^{2+}, then Mn^{2+}, in order to account for their different redox potentials (Armbruster et al. 2006). Similarly, the Fe^{2+}/Fe^{3+} and Mn^{2+}/Mn^{3+} values were calculated in spessartine, on the basis of 8 cations and 12 anions, and chemical data were recast into idealised site occupancies (Droop 1987; Grew et al. 2013).

Results

Macroscopic and textural characteristics of Mn nodules

In the fine-grained quartz and micaceous phyllite, synsedimentary nodules or elongated lenses up to 1 cm wide occur (Fig. 2a, b). Macroscopically, in the centre, they are light yellow, with up to 1 mm colourless quartz rims or fine veinlets penetrating the nodule matrix. Around them, a concentric up to 5 cm red to reddish-brown aureole is observed, fading gradually into the grey quartz–muscovite phyllite, formed by quartz, muscovite, albite, and titanite. Garnet is the primary mineral phase in nodules, while it forms a homogeneous yellowish compact central aggregate locally intersected by quartz veins. The transitional transparent zones consist of a fine-grained aggregate of quartz, clinochlore, and subhedral garnets. Peripheral parts of these yellowish garnet nodules are composed of fine-grained aggregates of quartz, isolated grains of garnet, epidote–piemontite, and accessory Mn-rich calcite forming the nodule's aureole. The red to reddish-brown colour of concentric aureole is mostly caused by the presence of hematite (Fig. 2a–d).

Mineralogical characteristics of nodules and Mn-rich aureole

Spessartine is the most common mineral in the studied manganese mineralisation. It occurs in two types. The first type is characterised by up to 1 cm wide light yellow nodules forming compact aggregates (Fig. 3a). It is intercepted by quartz veinlets and separated by quartz from the disseminated and isolated spessartine crystals in the peripheral transitional zone of spessartine nodule (Fig. 3a, b). The chemical composition of studied spessartine from nodules reaches values in the interval 78.9–90.5 mol.% (Table 1, Supplementary Table S1) and does not differ from the spessartine disseminated in the peripheral nodule zone (Fig. 4), with minor content of andradite (up to 10.0 mol.%), grossular (up to 9.5 mol.%), and other components (less than 1.0 mol.%). Locally, spessartine in nodules is zoned in the grain central parts (Fig. 3c), zoning is caused by an increase in andradite (up to 12.5 mol.%) or grossular (up to 12.1 mol.%; Table 1, Supplementary Table S1) components. The second type of spessartine occurs within the reddish aureole, where it occurs as subhedral isolated grains up to 50 μm in size (Fig. 3d). The chemical composition of this spessartine is similar to that in the disseminated peripheral zone, and it does not show visible zoning in BSE mode.

Epidote and ***piemontite*** are common minerals in the reddish aureole near the spessartine nodules, where they form a solid-solution series. They occur mostly within the quartz, muscovite, and albite matrix aligned with the host foliation, associated with spessartine, hematite, and rarely titanite. Both epidote-group minerals contain empty spaces and are porous or bear a significant amount of hematite inclusions. They show indistinct chemical zoning (Figs. 3d, 5a). The chemical

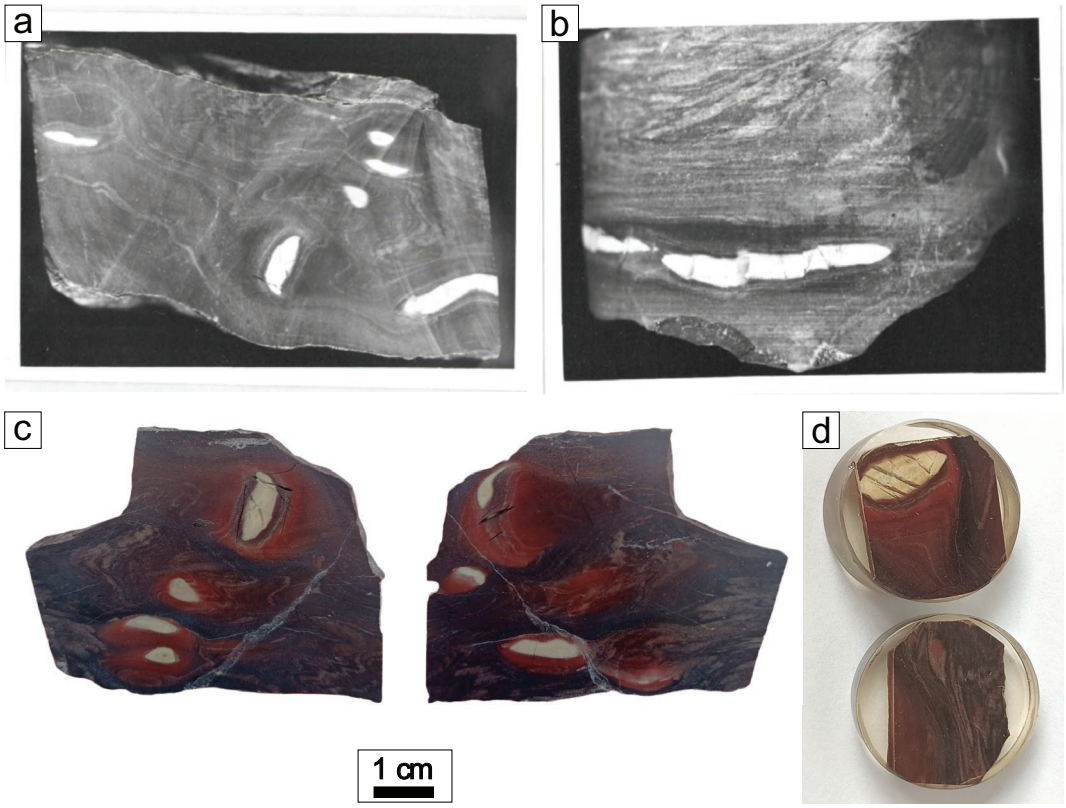

Fig. 2. (a, b) Original samples used during the study of Hudáček et al. (1984) from borehole RHV-1 obtained from the depth of 1280.2 m. The light lenticular lenses are composed of garnet and quartz. The distinctly "darker" pigmented rim of these lenses consists mainly of xenoblasts of epidote. Size of samples is approximately 6×3 cm; **(c)** sample deposited at the Department of Geography and Geology, Faculty of Natural Sciences of Matej Bel University in Banská Bystrica; **(d)** samples used in this study with light yellow garnet nodule intersected by quartz veinlets within the reddish Mn-rich aureole enriched in hematite, piemontite, epidote, spessartine and fluorapatite in phyllite, size 2.5×2.5 cm.

composition is shown in the classification diagram in Fig. 6, and two members of the epidote group are present: epidote (up to 97.1 mol.% Ep) and piemontite (up to 65.6 mol.% Pmt). The clinozoisite molecule is present only as a minor constituent up to 33.1 mol.%. Other, mostly minor constituents were also detected, e.g. Mn^{2+} (up to 0.38 *apfu*), Fe^{2+} (up to 0.12 *apfu*), Mg (up to 0.05 *apfu*), Cr, V, and Y (less than 0.01 *apfu*) (Table 2, Supplementary Table S1).

Hematite is a common mineral in manganese-rich aureole, as it mostly causes its reddish colour. Hematite forms fine-grained crystals and masses up to 80 µm in size; it also occurs in the form of inclusions in epidote, fluorapatite, titanite, and rarely in spessartine (Figs. 3c, d, 5a). Hematite was studied by SEM-EDS mode, and it shows no other constituents than Fe_2O_3.

Fluorapatite is an important accessory phase, as it was observed in two forms. The first form of fluorapatite (Fapt I) was observed in the spessartine nodule, where it forms anhedral crystals up to 20 µm in size in the form of inclusions, or it occurs in the interstitial places with spessartine. It shows not pronounced but frequent chemical zoning in BSE (Fig. 7a). The second form of fluorapatite (Fapt II) was observed in the Mn-rich reddish aureole (Fig. 7b), where it forms grains up to 50 µm in size (Fig. 7b, c, d). Zoning of this type of fluorapatite can be divided into two generations. The first – older one (Fapt I) is formed by homogenous, compact fluorapatite with monotonous chemical composition close to the ideal end-member formula (with As^{5+} reaching values close to the detection limit up to 0.02 *apfu*). The middle part of fluorapatite is porous and rich in hematite inclusions. Distinct zoning is similarly absent, but concentrations of As^{5+} rise with contents up to 0.07 *apfu*. The second generation (Fapt II) is mostly present in the peripheral parts, which are strongly zoned depending on As^{5+} and P^{5+} content (Fig. 8), with less hematite inclusions, as it shows the highest As^{5+}contents (up to 0.29 *apfu*) (Table 3, Supplementary Table S1). This second generation in the peripheral parts is chemically similar to the first type of fluorapatite in spessartine nodules.

Calcite is a rare phase that has only been identified in the form of fine-grained euhedral grains in spessartine nodules and at the quartz-rich disseminated spessartine area transitioning to the reddish Mn-rich aureole. It forms grains up to 10 µm in size (Fig. 5b) with indistinct zoning. The chemical composition shows dominant $CaCO_3$ (up to 90.4 mol.%), with slightly elevated content of Mn (up to 0.19 *apfu*), Mg (up to 0.03 *apfu*), and very low Fe and Sr (below 0.01 *apfu*). With decreasing content of Ca, the Mn and Mg increase, forming

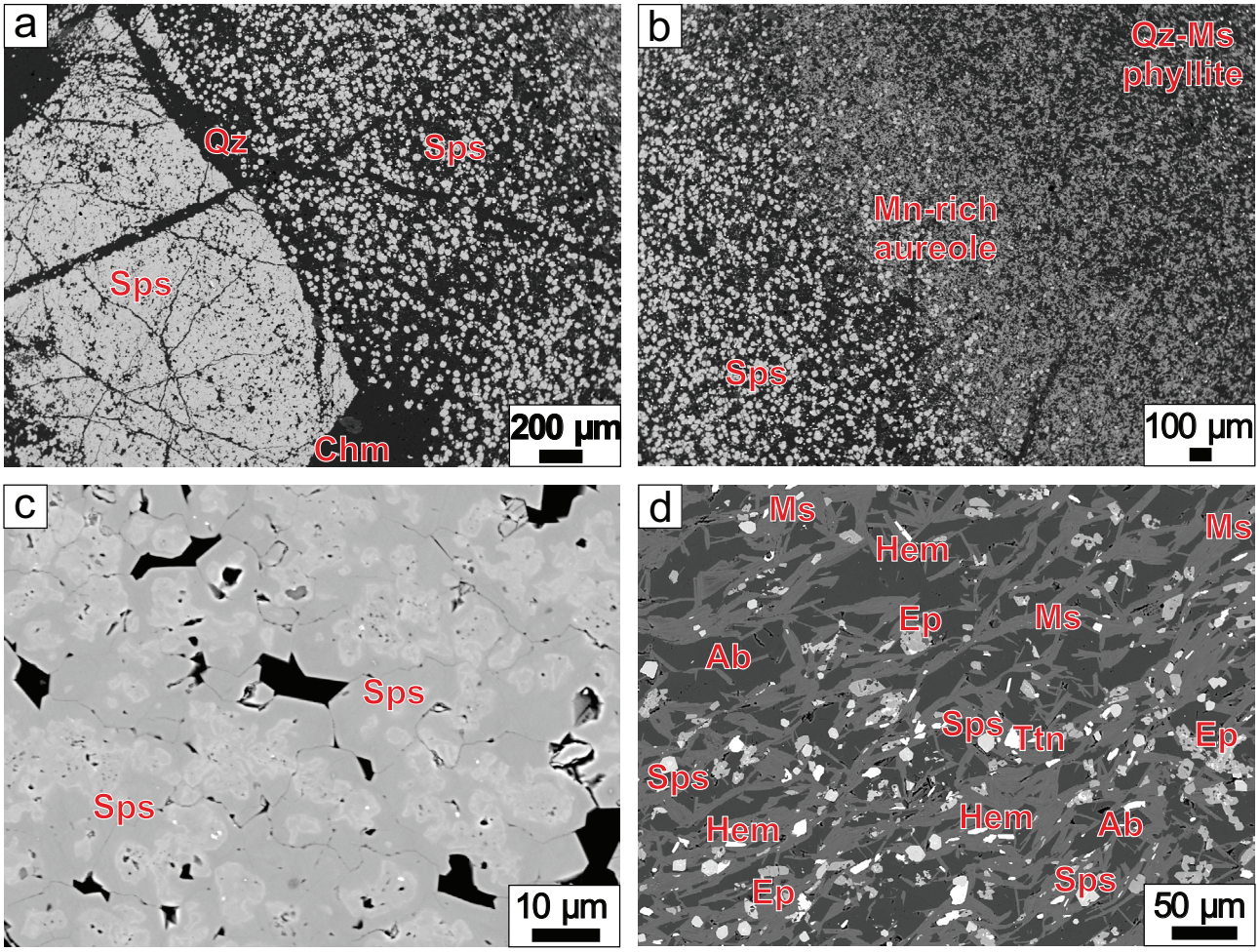

Fig. 3. (a) BSE images of spessartine nodule and the transitional disseminated quartz–spessartine zone; **(b)** transitional quartz–spessartine zone at the contact with aureole containing Mn-rich phases (Mn^{3+}-rich epidote, piemontite, spessartine etc.) and quartz–muscovite phyllite; **(c)** detail of zoned spessartine in the central part of a spessartine nodule; **(d)** detail of Mn-rich aureole containing grains of spessartine, epidote, piemontite, and hematite transitioning to quartz–muscovite phyllite with albite and titanite.

$MnCO_3$ component up to 20.1 mol.% with minor $MgCO_3$ up to 2.6 mol.% (Table 4, Supplementary Table S1).

Clinochlore was observed in the quartz zone between the spessartine nodule and the nodules aureole. It forms platy crystals grouped into the zoned aggregates (Fig. 5d). Zoning is caused by the substitution of Mg in darker BSE parts and Fe in lighter BSE parts, while it dominantly contains Mg^{2+} (up to 4.16 *apfu*) over Fe^{2+} (up to 0.39 *apfu*). The #Mg calculated as Mg/(Mg+Fe) is 0.79–0.91 (Supplementary Table S1).

Mineralogical characteristics of associated phyllites

Quartz forms the dominant part of quartz-muscovite phyllites, and it occurs as a late fracture-filling phase between the phyllite and manganese-bearing nodules. It was studied by SEM-EDS mode, and it shows no other constituents than SiO_2.

Muscovite is the dominant part of phyllites. It forms acicular elongated crystals perpendicular to the phyllite schistosity, with crystals generally 30–50 µm in size. It is closely associated with quartz and albite. The chemical composition shows indistinct contents of Mg^{2+} (0.37–0.61 *apfu*) and Fe^{2+} (0.17–0.32 *apfu*) at the *M*-site and dominant K^+ (0.91–1.04 *apfu*) at the *I*-site (Supplementary Table S1). In BSE mode, muscovite does not show any zoning (Figs. 3d, 4a,c, 6b–d).

Albite occurs widely as a part of phyllite matrix, where it forms anhedral grains associated with quartz and muscovite. Its chemical composition is monotonous with a dominant albite molecule (up to 99.7 mol.%) and minor anorthite (up to 0.6 mol.%) or orthoclase (up to 0.42 *apfu*) (Supplementary Table S1). In BSE, it shows no chemical zoning (Figs. 3d, 4a–c, 6b–d).

Titanite occurs rarely in the quartz-muscovite phyllites. It forms slightly zoned and porous subhedral grains (Fig. 5c). The chemical composition is close to the end-member formula with slightly increased Fe^{3+} (up to 0.05 *apfu*), Mg (up to 0.05 *apfu*), and Mn (up to 0.02 *apfu*), with minor Na and K (Supplementary Table S1). Anion site shows a slight increase in F^- content (up to 0.13 *apfu*).

Table 1: Representative chemical analyses of spessartine from RHV-1 borehole. Chemical formulae calculated on the basis of 8 cations and 12 oxygen atoms (*apfu*). Symbol * represents the calculation of Fe_2O_3 and Mn_2O_3 from the charge-balanced formula.

Analysis	**1**	**2**	**3**	**4**	**5**	**11**	**12**	**13**	**14**	**15**	**36**	**37**	**38**	**39**	**40**
Localisation	**nodule – central parts**					**nodule – outer parts**					**isolated crystals in matrix**				
SiO_2	35.71	35.45	36.18	35.34	34.19	35.85	35.39	35.71	35.88	35.75	35.03	35.20	35.38	35.08	35.18
TiO_2	0.18	0.16	0.05	0.10	0.26	0.12	0.20	0.11	0.00	0.05	0.09	0.00	0.00	0.09	0.00
Al_2O_3	18.69	18.35	19.07	17.96	17.37	19.03	18.29	18.28	19.11	19.15	19.11	19.74	19.82	19.84	19.91
Cr_2O_3	0.00	0.05	0.00	0.06	0.00	0.00	0.04	0.05	0.00	0.00	0.00	0.02	0.00	0.00	0.00
V_2O_3	0.00	0.04	0.00	0.02	0.04	0.00	0.11	0.05	0.03	0.00	0.04	0.02	0.00	0.00	0.00
Y_2O_3	0.00	0.00	0.00	0.00	0.03	0.00	0.00	0.09	0.00	0.03	0.00	0.00	0.03	0.00	0.00
Fe_2O_3*	2.30	3.07	1.98	3.38	3.78	2.17	3.25	2.86	1.99	1.48	0.96	0.61	0.75	0.61	0.67
Mn_2O_3*	0.80	2.37	1.02	1.80	3.91	1.03	1.57	0.79	1.88	1.20	3.08	3.82	2.18	2.82	3.32
MnO*	33.96	33.13	35.34	35.52	35.00	35.17	35.67	35.70	38.33	37.76	37.25	36.58	36.34	36.97	36.78
ZnO	0.00	0.00	0.04	0.00	0.00	0.00	0.00	0.00	0.03	0.00	0.00	0.00	0.09	0.00	0.00
MgO	0.04	0.02	0.05	0.02	0.00	0.07	0.13	0.03	0.02	0.06	0.05	0.09	0.13	0.10	0.11
CaO	6.55	6.97	5.77	4.94	4.43	5.54	4.80	5.15	3.15	3.47	3.25	3.81	4.04	3.44	3.60
Na_2O	0.00	0.00	0.00	0.00	0.00	0.03	0.00	0.00	0.00	0.00	0.00	0.00	0.00	0.00	0.00
Total	98.23	99.61	99.49	99.13	99.00	99.01	99.45	98.81	100.42	98.94	98.86	99.88	98.76	98.95	99.57
Zn^{2+}	0.000	0.000	0.002	0.000	0.000	0.000	0.000	0.000	0.002	0.000	0.000	0.000	0.006	0.000	0.000
Si^{4+}	2.974	2.925	2.979	2.946	2.876	2.967	2.937	2.976	2.952	2.973	2.924	2.901	2.937	2.915	2.906
Al^{3+}	0.026	0.075	0.019	0.054	0.124	0.033	0.063	0.024	0.046	0.027	0.076	0.099	0.057	0.085	0.094
Sum *Z*	3.000	3.000	3.000	3.000	3.000	3.000	3.000	3.000	3.000	3.000	3.000	3.000	3.000	3.000	3.000
Ti^{4+}	0.011	0.010	0.003	0.006	0.017	0.008	0.013	0.007	0.000	0.003	0.006	0.000	0.000	0.006	0.000
Al^{3+}	1.809	1.710	1.831	1.710	1.598	1.823	1.726	1.771	1.806	1.850	1.805	1.819	1.882	1.857	1.844
Fe^{3+}	0.144	0.190	0.123	0.212	0.239	0.135	0.203	0.180	0.123	0.093	0.060	0.038	0.047	0.038	0.041
Mn^{3+}	0.050	0.149	0.064	0.114	0.250	0.065	0.099	0.050	0.118	0.076	0.196	0.240	0.138	0.178	0.208
V^{3+}	0.000	0.003	0.000	0.002	0.002	0.000	0.008	0.003	0.002	0.000	0.003	0.001	0.000	0.000	0.000
Cr^{3+}	0.000	0.003	0.000	0.004	0.000	0.000	0.003	0.003	0.000	0.000	0.000	0.001	0.000	0.000	0.000
Mn^{2+}	0.000	0.000	0.000	0.000	0.000	0.000	0.000	0.000	0.000	0.000	0.000	0.000	0.000	0.000	0.000
Sum *Y*	2.015	2.065	2.021	2.048	2.106	2.030	2.050	2.014	2.050	2.022	2.070	2.099	2.067	2.080	2.094
Mn^{2+}	2.395	2.316	2.464	2.508	2.493	2.465	2.508	2.519	2.670	2.660	2.634	2.554	2.556	2.602	2.574
Mg^{2+}	0.005	0.003	0.006	0.003	0.000	0.009	0.015	0.004	0.003	0.007	0.006	0.011	0.016	0.012	0.014
Ca^{2+}	0.585	0.617	0.509	0.441	0.399	0.491	0.427	0.460	0.277	0.309	0.291	0.337	0.360	0.307	0.318
Na^{+}	0.000	0.000	0.000	0.000	0.000	0.005	0.000	0.000	0.000	0.000	0.000	0.000	0.000	0.000	0.000
Y^{3+}	0.000	0.000	0.000	0.000	0.001	0.000	0.000	0.004	0.000	0.001	0.000	0.000	0.001	0.000	0.000
Sum *X*	2.985	2.935	2.979	2.952	2.894	2.970	2.950	2.986	2.950	2.978	2.930	2.901	2.933	2.920	2.906
Spessartine	80.24	78.90	82.71	84.97	86.20	83.15	85.01	84.47	90.51	89.37	89.88	88.02	87.18	89.09	88.56
Pyrope	0.17	0.09	0.20	0.09	0.00	0.29	0.52	0.12	0.09	0.24	0.19	0.38	0.55	0.42	0.48
Grossular	12.06	10.72	10.83	3.75	0.83	9.53	3.32	5.91	3.02	5.63	6.53	9.53	9.87	8.38	8.82
Andradite	6.96	9.47	6.10	10.61	11.97	6.64	9.99	8.86	6.28	4.61	2.95	1.94	2.39	1.83	2.14
Schorlomite	0.57	0.51	0.16	0.30	0.87	0.39	0.64	0.34	0.00	0.15	0.29	0.00	0.00	0.29	0.00
Uvarovite	0.00	0.18	0.00	0.20	0.00	0.00	0.13	0.15	0.00	0.00	0.00	0.06	0.00	0.00	0.00
Goldmanite	0.00	0.13	0.00	0.08	0.13	0.00	0.38	0.15	0.10	0.00	015	0.07	0.00	0.00	0.00

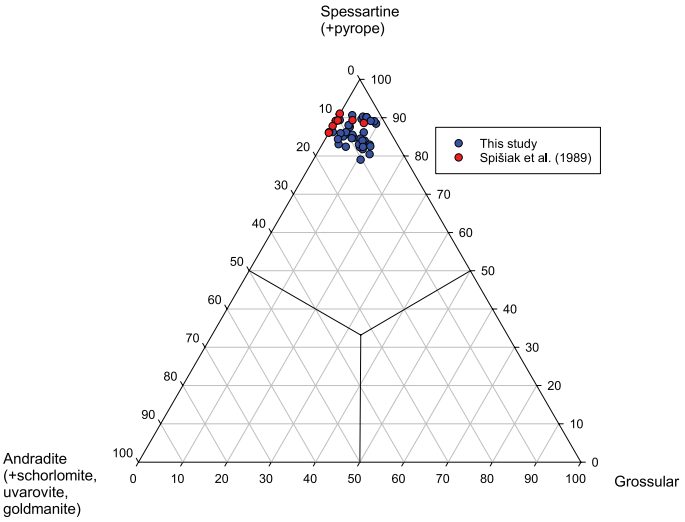

Fig. 4. Garnet supergroup minerals classification diagram with analyses from spessartine nodule and reddish aureole in the RHV-1 borehole from Spišiak et al. (1989) and this study.

Discussion

Polystadial development of manganese mineralisation in micaceous phyllites

The relatively simple manganese-rich mineral assemblage from the RHV-1 borehole near Rudňany indicates that mineralisation is strongly dependent on the host rocks, more precisely on the precursor material. The micaceous phyllites provide only a limited set of elements, causing minimal influence on the final composition of manganese mineralisation. The assemblage consisting of

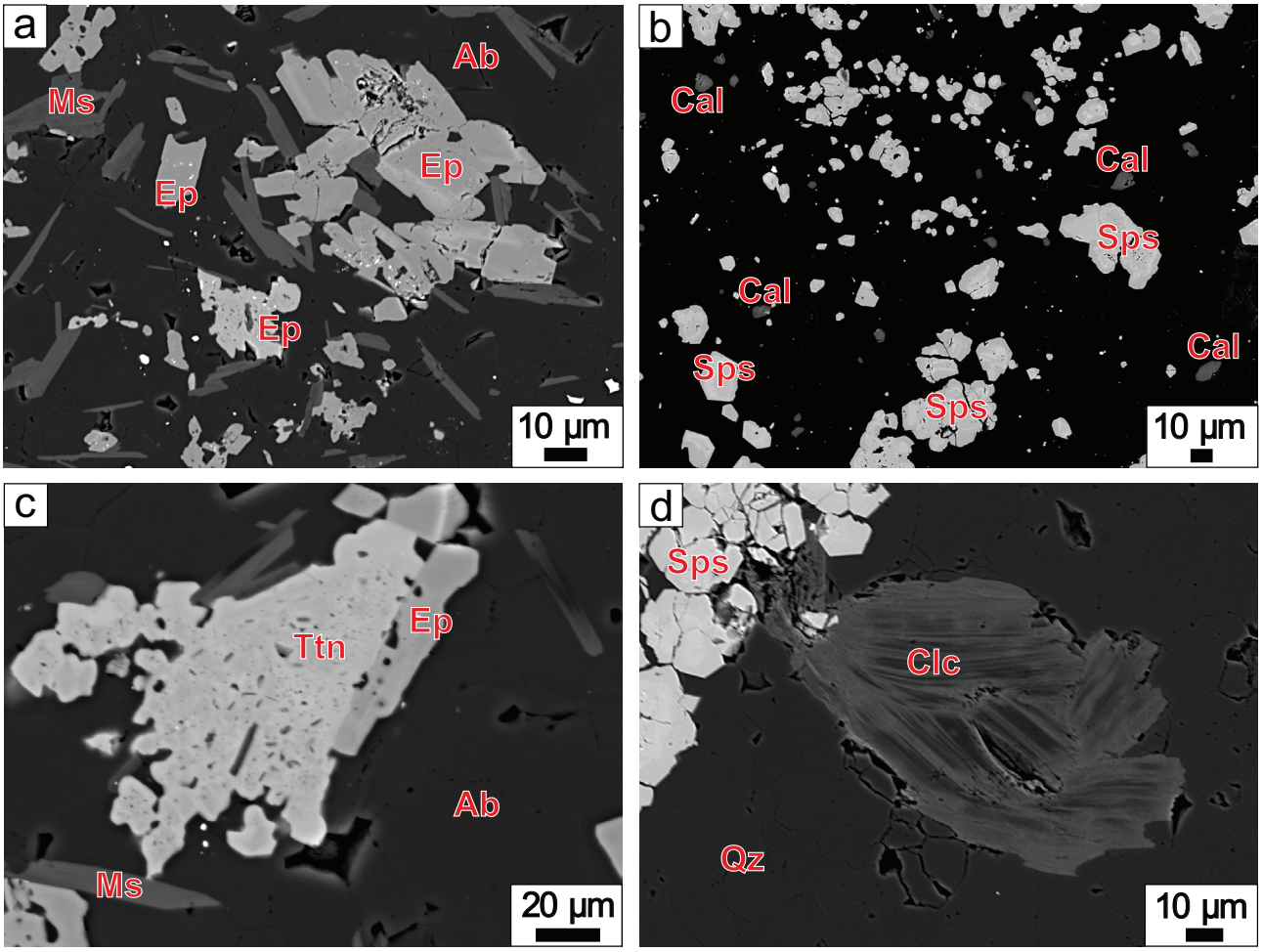

Fig. 5. (a) BSE images of epidote group minerals in Mn-rich aureole at the contact with quartz–muscovite phyllite with minor albite; **(b)** Mn-enriched calcite associated with spessartine grains in spessartine transitional zone near the spessartine nodule; **(c)** titanite crystals within Qz–Ms phyllite; **(d)** chamosite at the contact with spessartine nodule in the quartz–spessartine transitional zone.

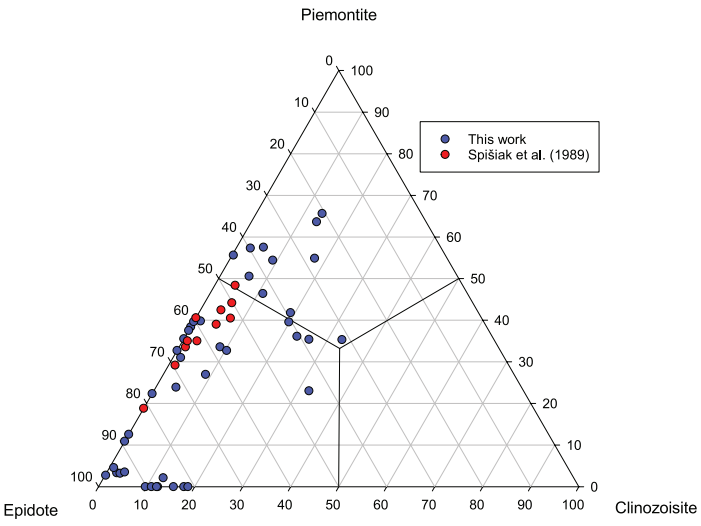

Fig. 6. Epidote group minerals classification diagram with analyses from Mn-rich zones in the RHV-1 borehole from Spišiak et al. (1989) and this study.

spessartine, epidote group minerals, hematite, quartz, and accessory calcite and fluorapatite may be considered predominantly "oxidic" (Mottana 1986). Mn-enrichment in calcite occurs only rarely. This interpretation is supported by the absence of organic matter and the probable accumulation of precursor Mn oxides and hydroxides within the pre-metamorphic manganese accumulations (Brusnitsyn 2017). As increasing fO_2 causes oxidisation of Fe^{2+} to Fe^{3+}, epidote, hematite, and the andradite component in spessartine becomes thermodynamically favoured. Similarly, Spišiak et al. (1989) emphasized that high oxygen fugacity (fO_2) represents a key factor in the formation of the observed mineral assemblage

The protolith of the micaceous phyllites was clayey–silty sediments containing variable amounts of volcaniclastic material. The presence of volcaniclastic products, together with sedimentary lamination, indicates the source of Mn precipitated through a volcanic source and its subsequent sedimentation in an Early

Table 2: Representative chemical analyses of epidote and piemontite from RHV-1 borehole. Chemical formulae calculated on the basis of (A+M+T)=8 cations (*apfu*) and 12.5 oxygen atoms. Symbol * represents the calculation of Fe_2O_3 and Mn_2O_3 from the charge-balanced formula. Symbol ** represents calculation of H_2O from (OH) = 1 *pfu*.

Analysis	1	2	3	4	5	6	7	8	39	40	41	47	48	49	50
Mineral	Epidote								Piemontite						
SiO_2	36.85	36.88	36.93	36.35	36.73	35.66	35.44	35.90	37.03	37.12	36.97	35.97	35.72	35.50	36.20
TiO_2	0.00	0.00	0.00	0.07	0.07	0.00	0.07	0.00	0.09	0.00	0.00	0.00	0.00	0.10	0.00
Al_2O_3	20.77	22.10	20.29	20.52	21.44	20.85	19.48	20.74	22.37	21.99	21.88	21.38	21.08	20.32	21.80
V_2O_3	0.00	0.00	0.00	0.00	0.00	0.00	0.02	0.00	0.00	0.00	0.00	0.00	0.04	0.00	0.04
Cr_2O_3	0.00	0.00	0.03	0.00	0.00	0.02	0.02	0.00	0.00	0.00	0.03	0.00	0.00	0.00	0.00
Fe_2O_3*	14.00	5.89	15.42	11.52	6.20	9.55	11.36	14.51	5.03	4.37	4.65	3.57	5.92	7.01	3.30
Mn_2O_3*	0.00	5.36	0.43	3.91	5.97	6.38	6.18	2.06	7.05	8.59	5.13	9.86	9.14	8.74	10.37
FeO*	0.41	0.00	0.00	0.00	0.00	0.00	0.00	0.00	0.00	0.00	0.00	0.00	0.00	0.00	0.00
MnO*	4.94	4.23	4.72	7.47	5.57	2.33	6.88	2.43	3.31	3.81	7.26	4.46	2.71	2.45	1.83
MgO	0.04	0.02	0.02	0.00	0.02	0.03	0.00	0.02	0.04	0.05	0.00	0.05	0.03	0.00	0.02
CaO	20.77	21.37	19.71	19.84	20.91	21.06	19.40	21.18	21.88	21.66	20.64	20.62	20.91	21.09	21.72
Na_2O	0.02	0.05	0.45	0.00	0.02	0.00	0.00	0.00	0.00	0.00	0.00	0.00	0.00	0.00	0.00
K_2O	0.00	0.00	000	0.00	0.00	0.04	0.02	0.04	0.00	0.00	0.00	0.03	0.09	0.04	004
Y_2O_3	0.03	0.03	0.00	0.04	0.00	0.00	0.00	0.02	0.06	0.10	0.00	0.00	0.00	0.04	0.00
H_2O**	1.81	1.80	1.81	1.81	1.80	1.80	1.79	1.81	1.83	1.83	1.78	1.79	1.79	1.78	1.81
Total	99.64	97.73	99.82	101.54	98.73	97.72	100.67	98.71	98.68	99.52	98.35	97.74	97.43	97.08	97.11
Ca^{2+}	1.812	1.862	1.715	1.761	1.830	1.882	1.745	1.879	1.923	1.898	1.795	1.854	1.874	1.901	1.931
Mn^{2+}	0.166	0.128	0.158	0.237	0.168	0.079	0.230	0.082	0.075	0.098	0.205	0.143	0.091	0.082	0.062
Na^{+}	0.003	0.008	0.071	0.000	0.003	0.000	0.000	0.000	0.000	0.000	0.000	0.000	0.000	0.000	0.000
K^{+}	0.000	0.000	0.000	0.000	0.000	0.005	0.003	0.004	0.000	0.000	0.000	0.003	0.009	0.005	0.004
Y^{3+}	0.001	0.001	0.000	0.002	0.000	0.000	0.000	0.001	0.003	0.004	0.000	0.000	0.000	0.002	0.000
Sum *A*	1.982	2.000	1.945	2.000	2.000	1.966	1.977	1.967	2.000	2.000	2.000	2.000	1.974	1.989	1.998
Ti^{4+}	0.000	0.000	0.000	0.004	0.004	0.000	0.005	0.000	0.005	0.000	0.000	0.000	0.000	0.006	0.000
Al^{3+}	1.993	2.119	1.943	2.003	2.064	2.024	1.902	1.996	2.162	2.120	2.093	2.114	2.065	2.001	2.132
Cr^{3+}	0.000	0.000	0.002	0.000	0.000	0.001	0.001	0.000	0.000	0.000	0.002	0.000	0.000	0.000	0.000
V^{3+}	0.000	0.000	0.000	0.000	0.000	0.000	0.002	0.000	0.000	0.000	0.000	0.000	0.003	0.000	0.002
Fe^{3+}	0.858	0.361	0.943	0.718	0.381	0.600	0.717	0.904	0.311	0.269	0.284	0.226	0.373	0.444	0.206
Mn^{3+}	0.000	0.332	0.027	0.247	0.371	0.405	0.395	0.130	0.440	0.535	0.317	0.630	0.582	0.560	0.655
Mg^{2+}	0.005	0.002	0.002	0.000	0.003	0.004	0.000	0.003	0.005	0.006	0.000	0.007	0.004	0.000	0.003
Fe^{2+}	0.028	0.000	0.000	0.000	0.000	0.000	0.000	0.000	0.000	0.000	0.000	0.000	0.000	0.000	0.000
Mn^{2+}	0.000	0.013	0.000	0.017	0.019	0.000	0.000	0.000	0.040	0.035	0.034	0.007	0.000	0.000	0.000
Sum *M*	2.884	2.826	2.916	2.989	2.842	3.034	3.023	3.033	2.963	2.964	2.729	2.983	3.026	3.011	2.998
Si^{4+}	3.000	3.000	3.000	3.011	3.000	2.974	2.975	2.973	3.037	3.036	3.000	3.017	2.987	2.986	3.004
Al^{3+}	0.000	0.000	0.000	0.000	0.000	0.026	0.025	0.027	0.000	0.000	0.000	0.000	0.013	0.014	0.000
Sum *T*	3.000	3.000	3.000	3.011	3.000	3.000	3.000	3.000	3.037	3.036	3.000	3.017	3.000	3.000	3.004
OH^{-}	1.000	1.000	1.000	1.000	1.000	1.000	1.000	1.000	1.000	1.000	1.000	1.000	1.000	1.000	1.000
Epidote	90.25	38.50	97.13	72.61	40.60	58.88	64.49	87.43	31.99	27.58	31.65	22.79	36.89	44.10	20.64
Clinozoisite	9.75	26.12	0.13	2.46	19.84	1,34	0.00	0.00	22.67	17.55	33.05	13.58	5.57	0.27	13.73
Piemontite	0.00	35.38	2.74	24.94	39.56	39.78	35.51	12.57	45.35	54.87	35.30	63.63	57.54	55.63	65.63

Paleozoic basin (Hudáček et al. 1984). This locally Mn-rich clayey and siliceous material was later transformed to muscovite, albite, and quartz. Ti-rich minerals (such as titanite) may represent original effusive or extrusive material with little or no admixture of sedimentary protolith, subsequently transformed during tectonometamorphic development.

The studied mineral assemblage indicates that the spessartine nodules developed within precursor sediments derived from Mn-enriched material of depositional mica or clay-rich layers, with minor limestone contribution. Locally accumulated calcareous components in the surrounding matrix likely promoted garnet formation during Variscan prograde metamorphic development under greenschist-facies conditions. Spessartine represents the main phase of the nodules and is considered the oldest mineral in the manganese assemblage as it formed during the prograde Variscan metamorphic stage at a relatively low-temperature environment (~300 °C). The low concentrations of temperature-sensitive cations (e.g., Ca, Mg, and Fe) in spessartine indicate equilibration at relatively low temperatures with minimal incorporation of these cations into the garnet structure during growth (Nyame 2001). The nodules contain marginal zones which likely represent transitional siliceous protolith material, while reddish rims are likely interpreted to have formed during syngenetic metamorphic recrystallisation. During this process, the nodules became oriented conformably with the host rock, often aligned with the host foliation. Subsequently, during the Alpine metamorphic event, the nodules were tectonically

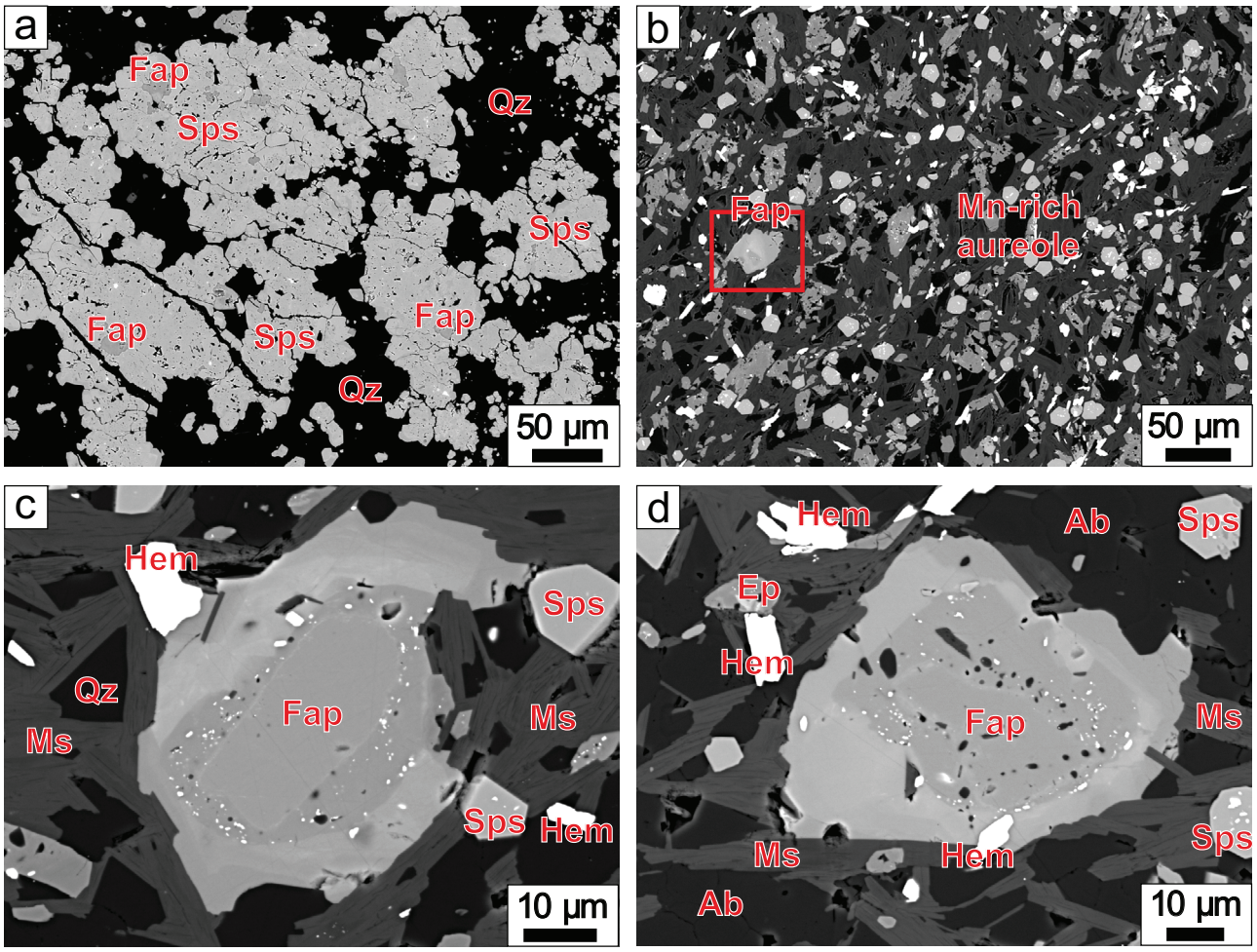

Fig. 7. (a) BSE images of As-rich fluorapatite in the spessartine aggregates within the spessartine nodule; **(b)** As-rich fluorapatite in Mn-rich aureole associated with epidote, piemontite, spessartine, and minerals from quartz–muscovite phyllite (quartz, muscovite, albite, titanite); **(c)** zonal fluorapatite (Fapt I) with As-poor central and intermediate zones enriched with As at the edges (Fapt II); **(d)** another fluorapatite grain with As-enriched zones along the edges.

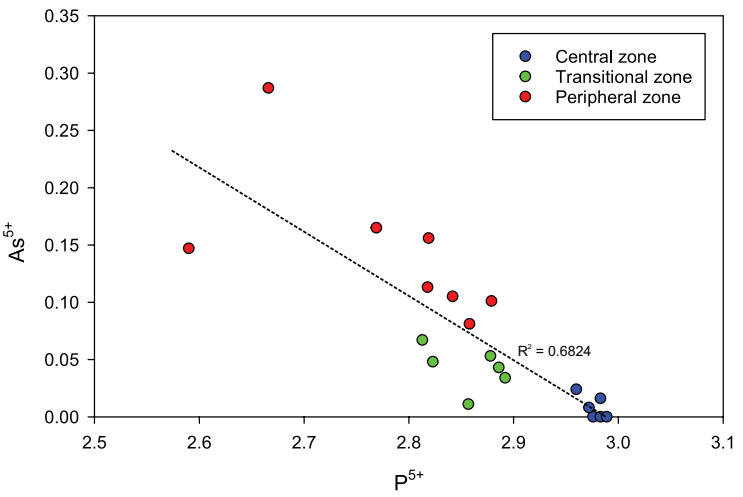

Fig. 8. As^{5+} vs. P^{5+} in *T*-site substitution diagram of zoned As-rich fluorapatite from Mn-rich aureole and spessartine nodule in the RHV-1 borehole, with calculated correlation coefficients R^2.

segmented and cut by quartz veinlets with clinochlore.

In contrast, metamorphic manganese mineralisation within the northern Gemeric Unit has been discovered and studied only at the Poráč occurrence (Myšľan et al. 2025b), where spessartine is a minor phase and the dominant garnets are andradite and grossular, together with their hydrated equivalents. The most notable difference between the Poráč occurrence and the Rudňany borehole assemblage is the absence of epidote-group minerals at Poráč, which otherwise form the dominant component of the manganese aureole at the studied samples. The presence of Fe^{3+} correlates with low Al^{3+} content, which might indicate a calderite component (Cenki-Tok & Chopin 2006).

The formation of piemontite is primarily controlled by elevated fO_2, although high manganese concentrations further expand its stability field.

Table 3: Representative chemical analyses of As-rich fluorapatite from RHV-1 borehole. Chemical formulae calculated on the basis of 8 cations (*apfu*) and 13 anions. F^- was normalised on 1 *apfu*. $Y+REE^{3+}=Y^{3+}+Ce^{3+}+La^{3+}+Nd^{3+}+Sm^{3+}+Pr^{3+}$.

Analysis	1	2	3	4	5	6	7	8	9	10	11	12	13	14	15
P_2O_5	40.66	40.71	40.66	38.91	40.81	38.77	39.55	38.93	39.86	39.56	38.80	35.73	38.58	37.80	36.19
As_2O_5	0.00	0.00	0.00	0.24	0.54	1.08	1.17	1.51	1.83	2.37	2.52	3.29	3.47	3.66	6.32
SiO_2	0.20	0.21	0.23	0.36	0.14	0.63	0.16	0.60	0.18	0.20	0.29	0.17	0.10	0.18	0.05
TiO_2	0.13	0.00	0.00	0.00	0.00	0.00	0.00	0.00	0.00	0.00	0.00	0.00	0.04	0.00	0.00
Al_2O_3	0.03	0.03	0.04	0.05	0.04	0.20	0.02	0.17	0.02	0.11	0.02	1.61	0.02	0.12	0.02
V_2O_3	0.04	0.05	0.04	0.00	0.00	0.00	0.00	0.00	0.00	0.00	0.00	0.00	0.00	0.04	0.03
Y_2O_3	0.00	0.00	0.03	0.00	0.00	0.02	0.02	0.04	0.04	0.00	0.00	0.00	0.00	0.00	0.00
Ce_2O_3	0.00	0.00	0.00	0.00	0.00	0.00	0.02	0.00	0.03	0.04	0.00	0.03	0.00	0.00	0.00
La_2O_3	0.00	0.00	0.00	0.00	0.00	0.02	0.00	0.00	0.00	0.00	0.00	0.04	0.00	0.00	0.00
Nd_2O_3	0.00	0.00	0.00	0.00	0.00	0.03	0.00	0.00	0.00	0.02	0.06	0.00	0.00	0.00	0.00
Sm_2O_3	0.00	0.00	0.00	0.00	0.00	0.00	0.00	0.00	0.00	0.02	0.00	0.00	0.00	0.00	0.00
Pr_2O_3	0.00	0.00	0.00	0.00	0.00	0.00	0.00	0.00	0.00	0.03	0.00	0.00	0.00	0.00	0.00
FeO	0.23	0.25	0.17	3.16	0.39	0.10	0.07	0.08	0.06	0.07	0.06	0.27	0.12	0.19	0.27
MnO	0.19	0.05	0.14	0.20	0.06	1.47	1.16	1.44	1.19	1.53	1.04	1.23	0.17	0.18	0.23
CaO	53.45	53.46	53.23	52.12	54.10	53.47	53.74	54.04	54.54	53.91	53.94	54.15	53.83	53.95	53.59
SrO	0.00	0.00	0.00	0.00	0.00	0.05	0.05	0.03	0.05	0.03	0.03	0.03	0.00	0.00	0.00
BaO	0.00	0.00	0.00	0.06	0.00	0.14	0.20	0.00	0.00	0.11	0.10	0.17	0.16	0.05	0.00
Na_2O	0.06	0.05	0.04	0.02	0.00	0.02	0.03	0.00	0.00	0.00	0.00	0.00	0.05	0.00	0.04
H_2O*	0.00	0.00	0.00	0.00	0.00	0.00	0.15	0.10	0.26	0.28	0.15	0.39	0.00	0.00	0.00
F	3.75	3.74	4.06	5.37	5.38	3.77	3.36	3.49	3.18	3.12	3.37	2.86	4.36	3.80	4.56
Cl	0.14	0.15	0.10	0.00	0.00	0.02	0.01	0.01	0.01	0.02	0.02	0.01	0.02	0.02	0.02
−O=F	−1.58	−1.57	−1.71	−2.26	−2.26	−1.59	−1.41	−1.47	−1.34	−1.31	−1.42	−1.21	−1.83	−1.60	−1.92
−O=Cl	−0.03	−0.03	−0.02	0.00	0.00	0.00	0.00	0.00	0.00	0.00	0.00	0.00	0.00	0.00	0.00
Total	97.27	97.10	97.00	98.24	99.21	98.18	98.29	98.96	99.90	100.10	98.96	98.77	99.05	98.39	99.37
P^{5+}	2.976	2.983	2.989	2.857	2.960	2.823	2.878	2.813	2.858	2.842	2.818	2.590	2.819	2.769	2.666
As^{5+}	0.000	0.000	0.000	0.011	0.024	0.048	0.053	0.067	0.081	0.105	0.113	0.147	0.156	0.165	0.287
Si^{4+}	0.017	0.018	0.020	0.031	0.012	0.055	0.014	0.051	0.015	0.017	0.025	0.015	0.008	0.016	0.004
Sum *T*	2.992	3.002	3.009	2.900	2.997	2.926	2.944	2.931	2.955	2.964	2.955	2.752	2.984	2.950	2.957
Ti^{4+}	0.009	0.000	0.000	0.000	0.000	0.000	0.000	0.000	0.000	0.000	0.000	0.000	0.003	0.000	0.000
Ca^{2+}	4.951	4.959	4.953	4.845	4.966	4.928	4.949	4.941	4.950	4.902	4.957	4.968	4.978	5.003	4.995
Fe^{2+}	0.017	0.018	0.012	0.229	0.028	0.007	0.005	0.006	0.004	0.005	0.004	0.019	0.008	0.014	0.020
Mn^{2+}	0.014	0.004	0.010	0.015	0.004	0.107	0.084	0.104	0.085	0.110	0.075	0.089	0.012	0.013	0.017
Sr^{2+}	0.000	0.000	0.000	0.000	0.000	0.002	0.002	0.002	0.002	0.001	0.002	0.002	0.000	0.000	0.000
Ba^{2+}	0.000	0.000	0.000	0.002	0.000	0.005	0.007	0.000	0.000	0.003	0.003	0.006	0.005	0.002	0.000
Na^+	0.010	0.009	0.007	0.004	0.000	0.003	0.005	0.000	0.000	0.000	0.000	0.000	0.008	0.000	0.006
Al^{3+}	0.003	0.003	0.004	0.005	0.004	0.021	0.002	0017	0.002	0.011	0.002	0.163	0.002	0.013	0.002
V^{3+}	0002	0.004	0.003	0.000	0.000	0.000	0.000	0.000	0.000	0.000	0.000	0.000	0.000	0.003	0.002
$Y+REE^{3+}$	0.002	0.002	0.002	0.000	0.000	0.001	0.001	0.000	0.001	0.003	0.002	0.002	0.000	0.002	0.001
Sum *M*	5.008	4.998	4.991	5.100	5.003	5.074	5.056	5.069	5.045	5.036	5.045	5.248	5.016	5.050	5.043
F^-	0.980	0.978	0.985	1.000	1.000	0.998	0.913	0.942	0.851	0.837	0.915	0.776	0.997	0.998	0.998
Cl^-	0.020	0.022	0.015	0.000	0.000	0.002	0.001	0.002	0.002	0.003	0.002	0.002	0.003	0.002	0.002
OH^-	0.000	0.000	0.000	0.000	0.000	0.000	0.085	0.057	0.147	0.160	0.083	0.223	0.000	0.000	0.000
Sum *A*	1.000	1.000	1.000	1.000	1.000	1.000	1.000	1.000	1.000	1.000	1.000	1.000	1.000	1.000	1.000

Consequently, piemontite typically occurs in highly oxidised, manganiferous sedimentary precursors that have undergone metamorphism under a wide range of p–T conditions. The most common precursor protoliths of piemontite-bearing rocks are cherts, corresponding to the altered oceanic floor sediments (Bonazzi & Menchetti 2004). The compositional and paragenetic characteristics of the piemontite-bearing assemblage indicate its formation predominantly under low- to intermediate-temperature metamorphic conditions. Substitution of Fe^{3+} for Mn^{3+} at *M*-sites is common and controlled by temperature, bulk-rock Fe^{3+}/Mn^{3+} ratios, and fO_2. Incorporation of Fe^{3+} generally extends the piemontite stability field toward lower fO_2 and higher temperature (Keskinen & Liou 1987).

Because both piemontite aggregates and garnet crystals display extensive solid-solutions involving Mn, Fe, and Al substitutions, the breakdown of piemontite and epidote may continuously proceed through a continuous equilibrium between coexisting epidote and garnet. In such a system, piemontite may continuously transfer Mn and Fe into the growing garnet structure as temperature increases or as fO_2 varies and vice versa (Bonazzi & Menchetti 2004). This assumption suggests that spessartine nodules within the studied samples may serve as early-formed phases providing key constituents for the subsequent metamorphic development of piemontite and epidote in the surrounding manganese aureole. The wide compositional zoning observed in the studied epidote and

Table 4: Representative chemical analyses of Mn-rich calcite from RHV-1 borehole. Chemical formulae calculated on the basis of 1 cation (*apfu*). The symbol * represents the calculated amount of CO_2 based on stoichiometry.

Analysis	1	2	3	4	5
CaO	42.81	45.04	47.26	48.19	50.33
MgO	1.25	1.04	0.82	0.38	0.37
FeO	0.00	0.06	0.07	0.00	0.14
MnO	12.95	10.63	9.02	8.26	5.24
SrO	0.06	0.00	0.00	0.02	0.00
CO_2*	43.02	43.11	43.62	43.37	43.24
Total	100.10	99.88	100.79	100.22	99.33
Ca^{2+}	0.781	0.820	0.850	0.872	0.913
Mg^{2+}	0.032	0.026	0.021	0.010	0.009
Fe^{2+}	0.000	0.001	0.001	0.000	0.002
Mn^{2+}	0.187	0.153	0.128	0.118	0.075
Sr^{2+}	0.001	0.000	0.000	0.000	0.000
Sum	1.000	1.000	1.000	1.000	1.000
$CaCO_3$	76.33	80.48	83.68	85.82	90.44
$MgCO_3$	2.62	2.17	1.71	0.79	0.79
$FeCO_3$	0.00	0.10	0.11	0.00	0.23
$MnCO_3$	20.97	17.25	14.50	13.35	8.54
$SrCO_3$	0.08	0.00	0.00	0.03	0.00

piemontite further reflects the wide range of chemical reactions within the spessartine-piemontite assemblage.

Fluorapatite serves as an important indicator of the multi-stage evolution of both the manganese mineralisation and the host micaceous phyllites. It is assumed that fluorapatite initially crystallised as an accessory phase within the phyllites, as evidenced by the presence of As^{5+}-poor cores, corresponding to a composition close to the ideal end-member formula of the first generation of fluorapatite (Fapt I). During the subsequent Variscan and Alpine metamorphic development under the greenschist-facies conditions, the fluorapatite underwent recrystallisation, forming porous transitional zones and new outer rims enriched in As^{5+} (up to 0.29 *apfu*) representing the second fluorapatite (Fapt II) generation. These newly formed fluorapatites were also generated in spessartine interstitial places within the nodules (Fig. 7a). The source of As within the system remains unclear, as arsenic may possibly originate from the volcanic source, inorganic matter within the protoliths of the phyllites, or it may have been remobilised during later Alpine tectonometamorphic overprint (Vozárová et al. 2013). Arsenic was observed only in minerals connected to the younger Alpine metamorphic development, with no evidence of its presence in the older Variscan-generated assemblage (e.g., epidotes) or in the associated host rocks.

Conclusions

The manganese nodules occurring within fine-grained quartz–muscovitic phyllites represent synsedimentary Mn-enriched precursors of siliceous, clayey, and partially calcareous sediment subsequently transformed by Variscan and Alpine metamorphism. Their internal zoning, characterised by spessartine cores, transitional quartz-spessartine zones and outer piemontite, epidote and hematite-bearing aureoles, reflects gradual mineral evolution with changing metamorphic grade. The nodules became structurally aligned with the host foliation during metamorphic deformation, which were later affected by Alpine tectonometamorphic segmentation and quartz vein formation. Spessartine represents the dominant manganese mineral with chemical composition (78.9–90.5 mol.% Sps), with minor andradite or grossular components crystallised at low-temperature greenschist-facies conditions. Minor zoning with grossular and andradite components reflects local changes in Ca and Fe content.

The reddish aureoles surrounding the spessartine nodules consist of epidote, piemontite, hematite, quartz, Mn-rich calcite, and fluorapatite, reflecting metamorphic redistribution of Mn^{3+} and Fe^{3+} under oxidising conditions. Piemontite crystallised from Mn-rich, oxidised fluid. Hematite contributed to the red coloration of the aureole. Fluorapatite occurs in two distinct generations: early As-poor fluorapatite enclosed in later As-enriched fluorapatite rims (up to 0.29 *apfu* As^{5+}) formed during recrystallisation under greenschist-facies metamorphism. The chemical zoning (As^{5+} up to 0.29 *apfu*) reflects multi-stage metamorphic and fluid evolution, with possible As^{5+} (re)mobilisation during the Alpine overprint.

Compared with other manganese occurrences in the northern Gemeric Unit (e.g., Poráč), the Rudňany assemblage is distinctive for its dominance of spessartine and the development of an epidote, piemontite, and hematite aureole. Overall, the mineralogical and chemical characteristics of the Mn nodules and aureoles point to a volcaniclastic-sedimentary origin subsequently modified by low-grade metamorphism and oxidising metamorphic fluids, representing a valuable record of Mn mobility and redox evolution of manganese mineralisation in the Gemeric Unit.

Acknowledgments: The authors are thankful to handling editor Peter Bačík as well as reviewers Bénédicte Cenki and Radek Škoda for their suggestions, which helped us to improve the manuscript. We are also thankful to P. Ivan, who provided us with samples, and F. Antalík for the sample photograph. This work was supported by the VEGA Grant No. 2/0029/23 and APVV-22-0041.

References

Armbruster T., Bonazzi P., Akasaka M., Bermanec V., Chopin Ch., GHieré R., Heuss-Assbichler S., Liebscher A., Menchetti S., Pan Y. & Pasero M. 2006: Recommended nomenclature of epidote-group minerals. *European Journal of Mineralogy* 18, 551–567. https://doi.org/10.1127/0935-1221/2006/0018-0551

Bajaník Š., Vozárová A. & Reichwalder P. 1981: Lithostratigraphic classification of Rakovec Group and Late Paleozoic sediments in the Spišsko-gemerské rudohorie Mts. *Geologické Práce, Správy* 75, 27–56 (in Slovak).

Bonazzi P. & Menchetti S. 2004: Manganese in monoclinic members of the epidote group: piemontite and related minerals. *Reviews in Mineralogy and Geochemistry* 56, 495–552. https://doi.org/10.2138/gsrmg.56.1.495

Brusnitsyn A. I., Starikova E. V. & Zhukov I. G. 2017: Mineralogy of low grade metamorphosed manganese sediments of the Urals: Petrological and geological applications. *Ore Geology Reviews* 85, 140–152. https://doi.org/10.1016/j.oregeorev.2016.07.004

Cenki-Tok B. & Chopin C. 2006: Coexisting calderite and spessartine garnets in eclogite-facies metacherts of the Western Alps. *Mineralogy and Petrology* 88, 47–68. https://doi.org/10.1007/s00710-006-0146-4

Cenki-Tok B., Ragu A., Armbruster T., Chopin Ch. & Medenbach O. 2006: New Mn- and rare-earth-rich epidote-group minerals in metacherts: manganiandrosite-(Ce) and vanadoandrosite-(Ce). *European Journal of Mineralogy* 18, 569–582.

Droop G.T.R. 1987: A general equation for estimating Fe^{3+} concentrations in ferromagnesian silicates and oxides from microprobe analyses, using stoichiometric criteria. *Mineralogical Magazine* 51, 431–435.

Faryad S.W. 1991: Pre-Alpine metamorphic events in Gemericum. *Mineralia Slovaca* 23, 395–402.

Faryad S.W. 1994: Mineralogy of Mn-rich rocks from greenschist facies sequences of the Gemericum, West Carpathians, Slovakia. *Neues Jahrbuch für Mineralogie* 10, 464–480.

Faryad S.W., Ivan P. & Jedlicka R. 2020: Pre-Alpine high-pressure metamorphism in the Gemer unit: mineral textures and their geodynamic implications for Variscan Orogeny in the Western Carpathians. *International Journal of Earth Sciences* 109, 1547–1564. https://doi.org/10.1007/s00531-020-01856-2

Grew E.S., Locock A.J., Mills S.J., Galuskina I.O., Galuskin E.V. & Hålenius U. 2013: Nomenclature of the garnet supergroup. *American Mineralogist* 98, 785–811. https://doi.org/10.2138/am.2013.4201

Hîrtopanu P. & Udubaşa G. 2015: Minerals from Răzoare Mn–Fe deposit, Preluca Mountains, East Carpathians: new data. *Romanian Journal of Mineral Deposits* 88, 11–28.

Hovorka D., Ivan P., Jilemnická L. & Spišiak J. 1988: Petrology and geochemistry of metabasalts from Rakovec (Paleozoic of Gemeric Unit, Inner Western Carpathians). *Geologický Zborník – Geologica Carpathica* 39, 395–125.

Hudáček J., Fabian M., Hrušovský S., Rényi K., Kufčáková A. & Cabalová K. 1984: Rudňany – deep boreholes, final report and resource calculation, raw material: complex iron ores, exploration survey, status as of August 1, 1984. *Manuscript, Geologický prieskum*, Spišská Nová Ves, 1–173 (in Slovak).

Ivan P. 2009: Early Palaeozoic basic volcanism of the Western Carpathians: geochemistry and geodynamic position. *Acta Geologica Universitatis Comenianae*, Comenius University, Bratislava, 1–110 (in Slovak).

Keskinen M. & Liou J. G. 1987: Stability relations of manganese-iron-aluminum piemontite. *Journal of Metamorphic Geology* 5, 495–507. https://doi.org/10.1111/j.1525-1314.1987.tb00398.x

Kolitsch U., Schachinger T. & Auer C. 2018: Aegirine, aegirine–augite, albite, baddeleyite, baryte, brandtite(?), braunite, calcite, canosioite, clino-suenoite (formerly "manganocummingtonite"), celestine, diaspore, dolomite, fluorapatite (containing As), fluorcalcioroméite, gamagarite, hematite, hausmannite, hjalmarite, hollandite, hydroxycalcioroméite, clinochlore, kutnohorite, mixed crystals manganiandrosite-(La)–manganiakasakaite-(La), nambulite, phlogopite, piemontite, pyrobelonite, Sb-containing pyrophanite, quartz, ranciéite(?), rhodochrosite, rhodonite, richterite, rutile, talc, thorite, tremolite, tilasite, titanite, tokyoite, wakefieldite-(Ce), wakefieldite-(Y), zircon, the Sb- analogue of hydroxymanganopyrochlore and unnamed $LaAsO_4$ from Obernberger Tribulaun, North Tyrol – the first report on mineralogically complex lens-shaped metamorphic manganese mineralisations. 206–213 In: Walter F. et al. 2018: New mineral discoveries from Austria LXVII. *Carinthia II*, 208/128, 185–254 (in German).

Mottana A. 1986: Blueschist-facies metamorphism of manganiferous chert: A review of the alpine occurrences. *Geological Society of America Memoirs* 164, 267–299.

Myšľan P., Števko M. & Mikuš T. 2023: Mineralogy and genetic aspects of the metamorphosed manganese mineralization at the Július ore occurrence near Betliar (Gemeric Unit, Western Carpathians, Slovakia). *Journal of Geosciences* 68, 313–332. https://doi.org/10.3190/jgeosci.384

Myšľan P., Števko M. & Mikuš T. 2024: Mineralogy of metamorphic magnetite-manganese ores at the Prakovce – Zimná Voda prospect (Spišsko-gemerské rudohorie Mts., Slovakia): The occurrence of REE-bearing allanite-subgroup minerals ferriakasakaite and ferriallanite. *Journal of Geosciences* 69, 231–249. https://doi.org/10.3190/jgeosci.400

Myšľan P., Števko M., Sejkora J., Ružička P. & Mikuš T 2025a: Metamorphic manganese mineralisation bound to the metacarbonate lenses at the Smolník – Malá Hekerová deposit in the Spišsko-gemerské rudohorie Mts., Western Carpathians (Slovakia). *Mineralogy and Petrology* 119, 243–258. https://doi.org/10.1007/s00710-025-00922-4

Myšľan P., Števko M., Mikuš T. & Vrtiška L 2025b: Mineralogy and genetic considerations of the metamorphosed As-rich manganese ore mineralization at the Diely occurrence near Poráč (Northern Gemeric Unit, Western Carpathians, Slovakia). *Mineralogical Magazine* 89, 71–91. https://doi.org/10.1180/mgm.2024.51

Nyame F. K. 2001: Petrological significance of manganese carbonate inclusions in spessartine garnet and relation to the stability of spessartine in metamorphosed manganese-rich rocks. *Contributions to Mineralogy and Petrology* 141, 733–746. https://doi.org/10.1007/s004100100257

Peterec D. & Ďuďa R. 2003: Rare minerals of Mn deposit near Čučma. *Natura Carpathica* 44, 229–236 (in Slovak).

Radvanec M. & Gonda S. 2020: Successive formation of Fe and Mn skarns in the Čučma locality (Gemeric unit, W. Carpathians): from metasomatic stage through the amphibolite facies overprint with Ti-rich tephroite to retrograde stilpnomelane-chlorite zone. *Mineralia Slovaca* 52, 103–132.

Rojkovič I. 2001: Early Paleozoic Manganese ores in the Gemericum Superunit, Western Carpathians, Slovakia. *Geolines* 13, 34–41.

Spišiak J. & Hovorka D. 2000: Piemontite and spessartine in Lower Paleozoic metasediments of the Inner Western Carpathians. *Acta Mineralogica-Petrographice, Szeged, XLI, Supplementum* 102.

Spišiak J., Hovorka D., Rybka R. & Turan J. 1989: Spessartine and piemontite in Lower Palaeozoic metasediments of the Inner West Carpathians. *Časopis pro mineralogii a geologii* 34, 17–29 (in Slovak with English summary).

Števko M., Plecháček J., Venclík V. & Malíková R. 2015: Hausmannite a manganosite from the Čučma-Čierna baňa manganese deposit (Slovak Republic). *Bulletin Mineralogie Petrologie* 23, 39–42.

Števko M., Myšľan P., Biagioni C., Mauro D. & Mikuš T. 2023: Ferriandrosite-(Ce), a new member of the epidote supergroup from Betliar, Slovakia. *Mineralogical Magazine* 87, 887–895. https://doi.org/10.1180/mgm.2023.62

Theye T., Schreyer W. & Fransolet A.M. 1996: Low-temperature, low-pressure metamorphism of Mn-rich rocks in the Lienne Syncline, Venn-Stavelot Massif (Belgian Ardennes) and the role of carpholite. *Journal of Petrology* 37, 797–783. https://doi.org/10.1093/petrology/37.4.767

Vozárová A. 1993: Te Variscan metamorphism in the Gemericum. *Geologické práce, správy, Abstracts of Scientific Reports*, 101, 16–18.

Vozárová A. & Šarinová K. 2024: Provenance of Upper Paleozoic sandstones from the Wetsern Carpathians (Slovakia): Petrofacies

analysis and U–Pb detrital zircon geochronology. *Geologica Caspathica* 75, 171–194. https://doi.org/10.31577/GeolCarp.2024.10

Vozárová A., Laurinc D., Šarinová K., Larionov A., Presnyakov S., Rodionov N. & Paderin I. 2013: Pb Ages of detrital zircons in relation to geodynamic evolution: Paleozoic of the northern Gemericum (Western Carpathians, Slovakia). *Journal of Sedimentary Research* 83, 915–927. https://doi.org/10.2110/jsr.2013.66

Vozárová A., Nemec O., Šarinová K., Anczkiewicz R. & Vozár J. 2021: Carboniferous mafic metavolcanic rocks in the Northern Gemeric Unit: Petrogenesis geochemistry, isotope composition and tectonic implication. *Geologica Carpathica* 72, 114–133. https://doi.org/10.31577/GeolCarp.72.2.3

Warr L. N. 2021: IMA-CNMNC approved mineral symbols. *Mineralogical Magazine* 85, 291–320. https://doi.org/10.1180/mgm.2021.43

Electronic supplementary material is available online:
Supplementary Table S1 at https://geologicacarpathica.com/data/files/supplements/GC-77-1-Myslan_TableS1.xlsx